J Solid State Electrochem (2011) 15:1169–1178
DOI 10.1007/s10008-010-1170-1

ORIGINAL PAPER

Activation energy for polypyrrole oxidation: film thickness influence

Toribio F. Otero · Jose G. Martinez

Received: 24 June 2010 / Revised: 4 August 2010 / Accepted: 5 August 2010 / Published online: 5 September 2010

Abstract The oxidation rates of polypyrrole films at different temperatures fit Arrhenius plots, allowing the obtention of the activation energy for the reaction. The activation energy increases for rising thicknesses, up to 4 μm, of the polymer film and decreases for rising film thicknesses. Those values include the constant chemical activation energy and the energy required to relax the polymeric structure allowing the entrance of anions from the solution. The existence of a maximum on the polymeric relaxation energy points to a parallel change on the film molecular structure during the electropolymerization time. The variation of the diffusion coefficient per degree of temperature for the counterions, as a function of the film thickness, is similar to that obtained for the activation energy. Diffusion coefficients were obtained from the electrochemical stretched exponential describing a range of relaxation behaviors in disordered and non-equilibrium systems.

Keywords Conducting polymers · Activation energy · Polypyrrole · Thickness · Diffusion coefficient · Stretched functions

Introduction

Oxidation and reduction reactions are produced by current flow through films of conducting polymers in presence of an electrolyte. During oxidation, every chain of the polymer film is transformed in a polymer salt, wearing rising number of positive charges uniformly distributed along the polymeric backbone and balancing counterions that penetrate from the solution. One of the reactant, the polymeric chains, located in a solid (or a dense gel) polymeric film and the other, the ions, in the electrolyte.

During oxidation reactions, under prevalent interchange of anions, the film swells. During reduction the film shrinks. Dimensional changes, or volume variations in films of conducting polymers, have been followed by different methodologies, or estimated from experimental densities and weights of the dried oxidized and reduced films, in some of the pioneering works of the electrochemistry of conducting polymers [1–13]. Those changes were confirmed at microscopic level by "in situ" AFM, ellipsometry, or in situ electrogravimetry [14–19]. Based on those volume changes, new electro-chemo mechanical actuators, or artificial muscles, are being developed from 1992 [20–25].

Those complex processes induced by the reaction are being modelized by the electrochemically stimulated conformational relaxation model [26–31]. This self-consistent model (without adjustable parameters) tries to integrate electrochemistry, polymer science, mechanics, and thermodynamics.

According with this model, films of conducting polymers having a prevalent interchange of anions between the film and the solution during reaction shrink during reduction. The structure is closed still under partial oxidation trapping up to 40% [32] of the counterions present under full oxidation state. The reduction and packing of the conformational structure by expulsion of the remaining counterions becomes slower. Reproducible reduced and packed states can be obtained, starting from an oxidized material, by reduction at the same cathodic potential for the same reduction time.

Electronic supplementary material The online version of this article (doi:10.1007/s10008-010-1170-1) contains supplementary material, which is available to authorized users.

T. F. Otero (✉) · J. G. Martinez
ETSII, Center for Electrochemistry and Intelligent Materials (CEMI),
Universidad Politécnica de Cartagena,
Paseo Alfonso XIII, Aulario II,
30203 Cartagena, Spain
e-mail: toribio.fotero@upct.es

Any subsequent oxidation by anodic potential steps gives chronoamperograms showing a maximum (Fig. 1). By integration, the evolution of the consumed charge (Q vs. t) with time is obtained. From the polymer weight (w) and the Faraday constant (F, C mol^{-1}) the evolution of the counterion concentration, as specific concentration, [$Q/(Fw)$, mol g^{-1}] in the film during oxidation is obtained, giving the oxidation kinetics: variation of the counterion concentration with time. Those are kinetics having an induction time. Taking slopes at the induction time for different reactant concentrations or different temperatures as initial oxidation rates the reaction is proved to occur under chemical kinetic control [33–37].

The attained rate constant, or rate coefficient, results a function of the conformational packing initial state used for the oxidation and obtained by electrochemical reduction at different cathodic potentials for the same reduction time [33]. The activation energy, obtained in a similar way, includes two components: the chemical activation energy of the reaction plus the conformational energy of the initial reduced and packed state [34–36].

On the other hand, the influence of thickness of conducting polymer films on corrosion protection [38, 39] for smart windows [40, 41], related to electrical [42–45] and electrochemical [46–51] properties, or for sensor responses [52–56] has been previously presented. The standard rate constant (k_o) for electron-transfer between Pt/PEDOT(PSS) and $Fe(CN)_6^{3-/4-}$ decreases very fast for increasing film thicknesses [57]. Similar results were obtained for the oxidation rate constants of PEDOTH [58] also for polyaniline, poly(*o*-methylaniline), and poly(*o*-methoxyaniline) [40]. Strain measurements and strain rate changes during oxidation/reduction also present great changes for film thicknesses changing from the nanometer to the micrometer range [59].

Here, by using chemical kinetic methodologies, we will try to obtain and to analyze the activation energy of the reaction from polymer films having different film thickness.

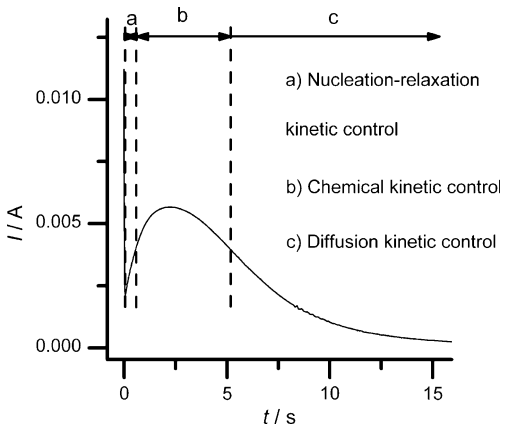

Fig. 1 Chronoamperometric response for a 2.65-μm thick polypyrrole film in 0.1 M $LiClO_4$ acetonitrile solution after reduction at −1,200 mV at room temperature for 60 s and subsequent oxidation at 18°C by potential step to 200 mV. Three different regions are indicated with the concomitant kinetic control process: *a* nucleation-conformational relaxation kinetic control, *b* chemical kinetic control, and *c* diffusion kinetic control

Experimental

All the electrochemical experiments were performed using a potentiostat-galvanostat Autolab PGSTAT100. Pyrrole (Fluka) was purified by distillation under vacuum at 20 mbar, using a diaphragm vacuum pump MZ 2C SCHOTT. Once distilled, it was stored at −15°C. Acetonitrile (Panreac, purity (HPLC) >99.9%) and lithium perchlorate (Aldrich, purity >98%) were used as received. A platinum electrode having 1 cm^2 surface area (0.5 cm^2 plate) was used as working electrode and, a stainless steel plate having 4 cm^2 of surface area was used as counter electrode. The reference electrode was a Metrohm of Ag/AgCl (3 M KCl) electrode. Ultrapure water was obtained from Milli-Q equipment.

Polypyrrole films were electrochemically obtained from 0.1 M $LiClO_4$ and 0.1 M pyrrole acetonitrile solution with 1% of water content, by flow of different anodic polymerization charges (to obtain different film thicknesses) through the working electrode, under polarization at a constant potential of 900 mV vs. Ag/AgCl (3 M KCl). After polymerization, the coated electrode was rinsed with acetonitrile. The weight of the dry electrogenerated film was obtained from a Sartorious SC2 balance having a precision of 10^{-7} g. The morphology of the obtained films, and the film thickness, was obtained by scanning electron microscopy (SEM Hitachi S-3500 N, 5 kV, 106 μA electron energy, and 30% beam current). When the temperature was studied, the temperature of the cell was maintained by means of a Julabo F25 cryostat (±0.1°C). All the other experiments were performed at room temperature.

The study of the oxidation reactions and the electrochemical control of the films were performed in 0.1 M $LiClO_4$ acetonitrile solution after de-aeration by N_2 bubbling for 10 min before each experiments. Every new film was checked by cyclic voltammetry in the 0.1 M $LiClO_4$ acetonitrile solution between −700 and 300 mV vs. Ag/AgCl, at 50 mV s^{-1}. The voltammetric control was repeated after potentiostatic steps to ensure that the polymer film has not deteriorated. Before initiating the kinetic experiments, the polymer film was submitted to several potential steps to ensure the steady-state chronoamperometric response. When the film was degraded, a new film was electrogenerated; a new experimental series was started, and the previous results were repeated.

Results and discussion

Polypyrrole films were electrogenerated on clean platinum electrodes from 0.1 M $LiClO_4$ plus 0.1 M pyrrole and 1% Milli-Q water, acetonitrile solutions by a potential step from 0 to 900 mV at room temperature. The different thicknesses were attained by keeping the oxidation times required to flow increasing polymerization charges: 150, 300, 450, 600, 675, 750, 900, 1,200, 1,400, 1,600, and 1,650 mC (The times of generation are different for different thicknesses). Those charges were obtained by integration of the experimental chronoamperograms recorded during film generations (see Supplementary information).

Once rinsed with acetonitrile and dried, the weights of every film was obtained using a SARTORIOUS SC2 balance. If we assume a uniform film, the thickness can be calculated:

$$h = w/(S\rho) \tag{1}$$

where h is the thickness of the polymer film, w is the film weight, S is the area of the working electrode, and ρ is the polypyrrole density (ρ=1.54 g cm^{-3}) [20].

The film thicknesses were checked by scanning electron microscopy (SEM Hitachi S-3500 N). From different films weighing 0.1204, 0.2279, 0.6803, and 0.8373 mg having a calculated average thickness (calculated from Eq. 1) of 0.78, 1.48, 4.41, and 5.43 μm, respectively, micrographic thicknesses of 0.56 (Fig. 2a), 1.3 (Fig. 2b), 4.15 (Fig. 2c), and 5.64 μm (Fig. 2d) were obtained. Thickness calculated from the polymer weight and those measured from the SEM results are quite similar.

As it should correspond to a Faradic electrogeneration, a good linear relationship exists between the thickness of the electrogenerated films, calculated from the film weight according to Eq. 1 (Supplementary information) and the charge consumed during the electrogeneration [60]. The charge consumed to obtain 1 mg of material of 2.28 C/mg was obtained.

Electrochemical control of the electrogenerated films

Once electrogenerated, the oxidation reaction of the electrogenerated films was studied. The electrochemical behavior, or electroactivity, of polypyrrole in $LiClO_4$ acetonitrile (AN) solutions can be summarized, in a simplified way, as:

$$\left[\mathrm{pPy}^{a+}(\mathrm{ClO_4}^-)_a\right]_s + n(\mathrm{ClO_4}^-)_{\mathrm{sol}} + m(\mathrm{AN}) \leftrightarrows \left[\mathrm{pPy}^{(n+a)+}(\mathrm{ClO_4}^-)_{n+a}(\mathrm{AN})_m\right]_{\mathrm{gel}} + n(e^-)_{\mathrm{metal}} \tag{2}$$

where the different sub-indexes mean: *s*, solid and *sol*, solution and pPy represents the active center on the neutral polypyrrole chains that will participate on the oxidation reaction storing a positive charge at the end of the reaction. The term $[\mathrm{pPy}^{a+}(\mathrm{ClO_4}^-)_a]_s$ indicates the difficulty to get a totally reduced material. The number of positive charges a indicates the difficulty to obtain a totally reduced film.

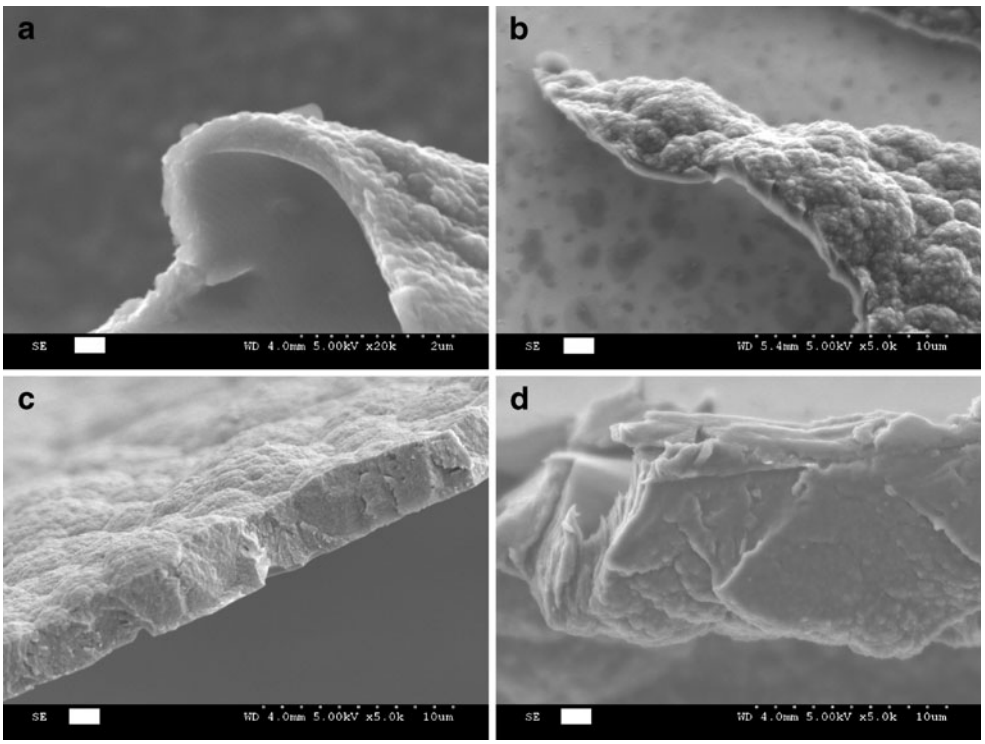

Fig. 2 SEM micrographs from polypyrrole films electrogenerated by flow of **a** 225, **b** 450, **c** 900, and **d** 1,600 mC

Rising packed initial states will promote decreasing values of a. The electrochemical oxidation corresponds to the forward reaction, and the electrochemical reduction corresponds to the backward reaction.

The electrochemical activity of each electrogenerated film was checked by voltammetric and by chronoamperometric controls in 0.1 M $LiClO_4$ acetonitrile solutions. Control voltammograms for increasing polypyrrole thickness were obtained between −700 and 300 mV vs. Ag/AgCl at 10 mV s^{-1} at room temperature (see Supplementary information). Increasing areas, which means rising charges, are involved in both, oxidation (positive currents) and reduction (negative currents) processes from films of rising thickness. In the same solution, the electrochemical activity of the films also was checked by potential steps from −1,200 mV, kept for 60 s to 200 mV.

By integration of the anodic chronoamperograms, or the anodic voltammograms, the charge consumed during oxidation of the polymer films was obtained. Supplementary information shows the linear increase of the charge required to oxidize the film as a function of the charge consumed during the polymerization process or of the film thicknesses. The expected result for the combination of two Faradic processes is obtained: electrogeneration of the films (constant charge to generate one weight unit of the polymer films) and electrochemical activity of the attained films (constant charge required to oxidize one weight unit of the polymer films).

Oxidation kinetics and activation energy

The oxidation rate, according with Eq. 2 should be expressed as:

$$r = Ae^{(-Ea/RT)}[ClO_4^-]^{\alpha}\left[pPy^*\right]^{\beta} \tag{3}$$

where r represents the oxidation rate of the polymer; $Ae^{(-Ea/RT)}$ is the rate constant or rate coefficient, K; A is the pre-exponential factor, E_a is the activation energy, R is the universal gas constant (R=8.314 J K^{-1} mol^{-1}), and T is the temperature; and α and β are the reaction orders and [pPy^*] is the concentration of active centers in the film, understood as those points on the chains where a positive charge will be stored after oxidation. The oxidation rate r, as mol s^{-1} cm^{-3}, can be obtained at any reaction time from the experimental charge Q (C) flowing through the electrode during a time t, the electrode area, S (cm^2), the Faraday constant F (96,485 C mol^{-1}), and the film thickness, h (cm):

$$r = Q/(tFSh)\text{mols}^{-1}\text{cm}^{-3} \tag{4}$$

And taking into account that $Q/(t{\cdot}S)$ is the current density, i (mA cm^{-2}) a second expression for the oxidation rate, as function of the current density flowing during oxidation through the coated electrode is obtained:

$$r = i/(Fh) \tag{5}$$

Considering the polymer weight of every studied film, the reaction rate also could be expressed as a function of the specific current, j (mA mg^{-1}). From Eq. 4 and considering that the product Sh is the film volume:

$$r = Q/(tFV) = Q\rho/tFw = i\rho/Fw = j\rho/F \tag{6}$$

Coming back to Eq. 3 and by taking logarithms:

$$\ln r = \ln A - E_a/RT + \alpha \ln[ClO_4^-] + \beta \ln\left[pPy^*\right] \tag{7}$$

So, under chemical kinetic control a semilogarithmic relationship should be expected from Eq. 7 between the reaction rates and T^{-1}:

$$\ln r = k - E_a/RT \tag{8}$$

where $k = \ln A + \alpha \ln[ClO_4^-] + \beta \ln\left[pPy^*\right]$.

Equation 7 indicates the experimental procedure that must be followed to obtain the activation energy: every film must be submitted to oxidation reactions at different temperatures from the same initial reduced state and keeping constant either, [ClO_4^-] (them, αln [ClO_4^-], will be constant) and [pPy^*] (the term, β ln [pPy^*], will become constant). Experimental results obtained from films having different thicknesses only could be compared if the potentiostatic oxidation always starts from the same initial state. With this aim, all the films were oxidized and swollen at 200 mV for 30 s at ambient temperature in order to erase structural memory from any previous treatment. Then they were reduced by potential step to −1.20 V for 60 s to get a similar initial reduced and packed structure for the subsequent oxidation. Both, reduction potential and reduction time are high enough to get a similar reduced (see reduction chronoamperograms at the Supplementary information) and packed conformational structure every time.

In order to check Eq. 8, the electrode, once reduced and packed at ambient temperature, was lifted from the solution into the nitrogen atmosphere of the closed cell and the bath was adjusted to the working temperature. When the cell solution attains this temperature, the coated electrode was returned into the solution and submitted to the oxidation potential step: from the initial state, readapted now by prepolarization at −1,200 mV for 1 s to 200 mV vs. Ag/AgCl. The procedure of reducing and packing at ambient temperature and oxidation at the working temperature was repeated for every film at different temperatures.

Figure 3 shows the experimental oxidation chronoamperograms obtained at −10°C, −3°C, 4°C, 11°C, 18°C, 25°C, and 32°C from each of the films thicknesses of 0.67, 1.88, 3.47, and 5.41 μm.

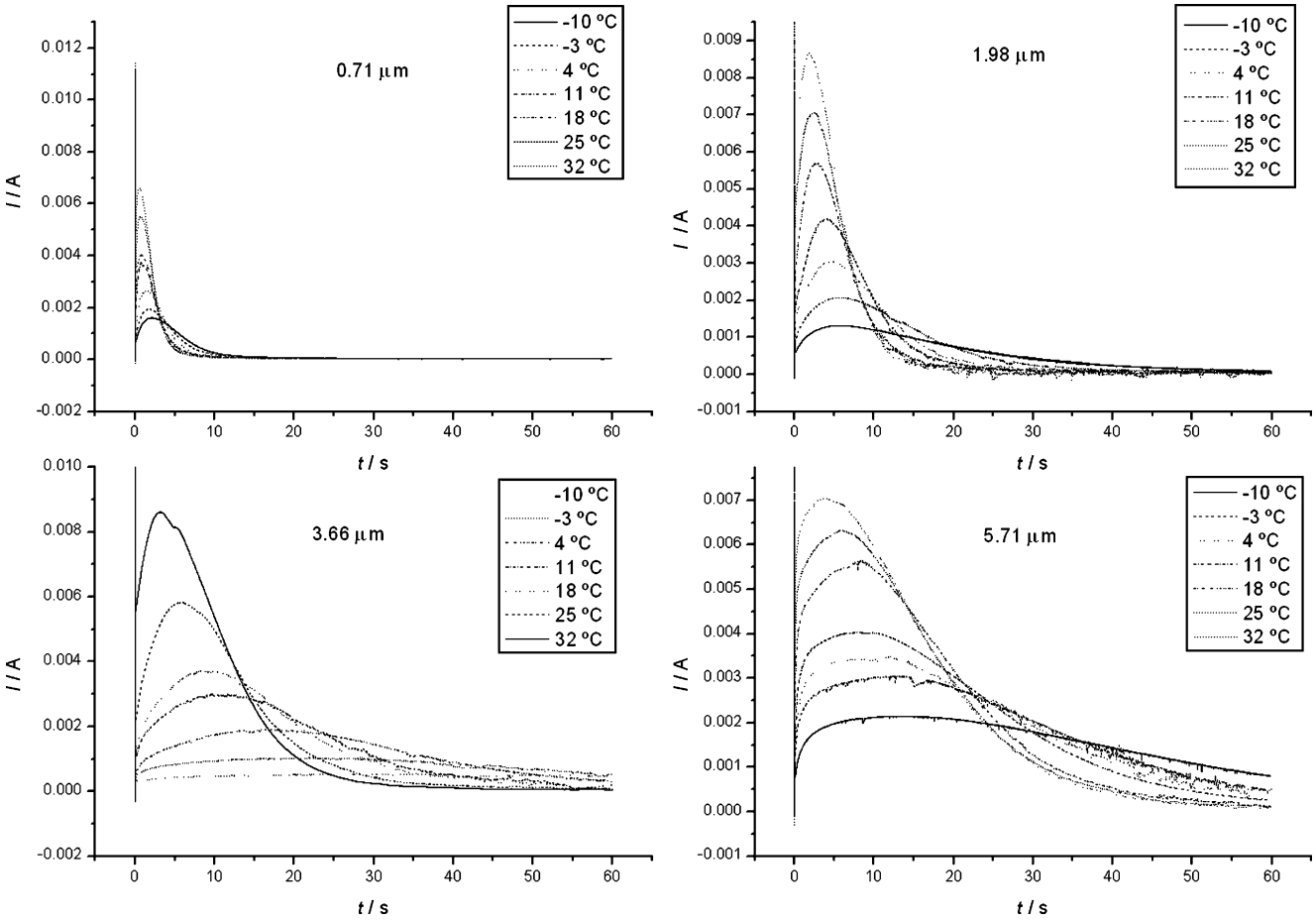

Fig. 3 Chronoamperometric responses for polypyrrole films in 0.1 M $LiClO_4$ acetonitrile solution. The coated electrode was reduced every time at −1,200 mV at room temperature for 60 s, then the electrode was extracted from the solution into the nitrogen, and the cell temperature was adjusted to a different temperature every time: −10°C, −3°C, 4°C, 11°C, 18°C, 25°C, or 32°C. The electrode was then put back into the solution and submitted to the potential step from −1,200 mV, kept for 1 s, to 200 mV vs. Ag/AgCl kept 60 s and then reduced at −500 mV. The procedure was repeated for different film thicknesses (0.67, 1.88, 3.47, and 5.41 μm)

All the chronoamperometric responses show a maximum after the initial sharp peak corresponding to the charge of the electrical double layer (polymer/solvent and polymer/metal). By integration of those responses, the chronocoulograms (Supplementary content) were obtained, representing the oxidation kinetics. Those are kinetics having an induction time obtained by intersection of the slope at the inflection point with the abscise axe. That slope, dQ/dt, is the initial oxidation rate that we are looking for in order to check Eq. 8 [34, 61]. The slope at the inflection point of the chronocoulogram is the current at the chronoamperometric maxima.

In order to adjust dimensions, those currents are transformed to the reaction rates using Eq. 5. Finally, from the experimental results for the different studied thicknesses, a semilogarithmic variation of the reaction rate at the chronoamperometric maxima, as a function of (1/T) (Fig. 4), was obtained.

All the experimental Arrhenius plots (Eq. 8) present high correlation coefficients (>0.95). The concomitant activation energies for the different film thicknesses are obtained from the slopes.

Two different trends can be observed. The activation energy increases for rising thicknesses of the film up to 4 μm (Fig. 5a). From there the activation energy decreases for increasing thicknesses of the polypyrrole film. By combining Eqs. 4 and 8:

$$E_a = K' - RT\ln(1/h),\ \text{or},\ E_a = K'' - RT\ln(1/w) \qquad (9)$$

where $K' = kRT - RT\ln[Q/(tFS)]$ or $K'' = kRT - RT\ln[Q\rho/tF]$.

Figure 5b shows a semilogarithmic plot between the inverse of the thickness and the obtained activation energy.

Kinetic results indicate the presence of two different processes or structures inside the material [62]. By impedance measurements, an important change on the relaxation characteristic frequency also was found in polypyrrole films after a polymerization charge of 60 mC (3 μm) on ITO [63]. The apparent diffusion length

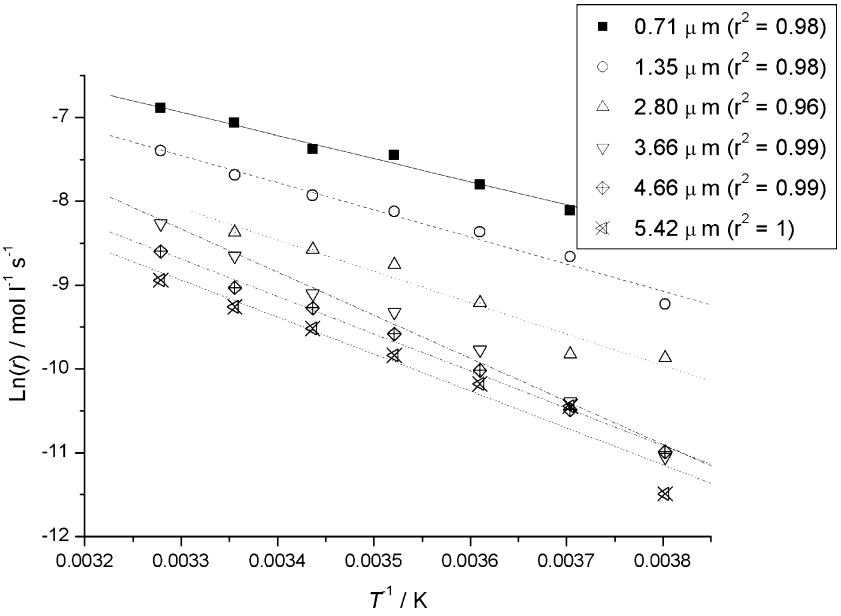

Fig. 4 Arrhenius plot for the polypyrrole oxidation in 0.1 M $LiClO_4$ acetonitrile solution at −10°C, −3°C, 4°C, 11°C, 18°C, 25°C, and 32°C, for some of the different studied thicknesses. Correlation coefficients r^2 are shown

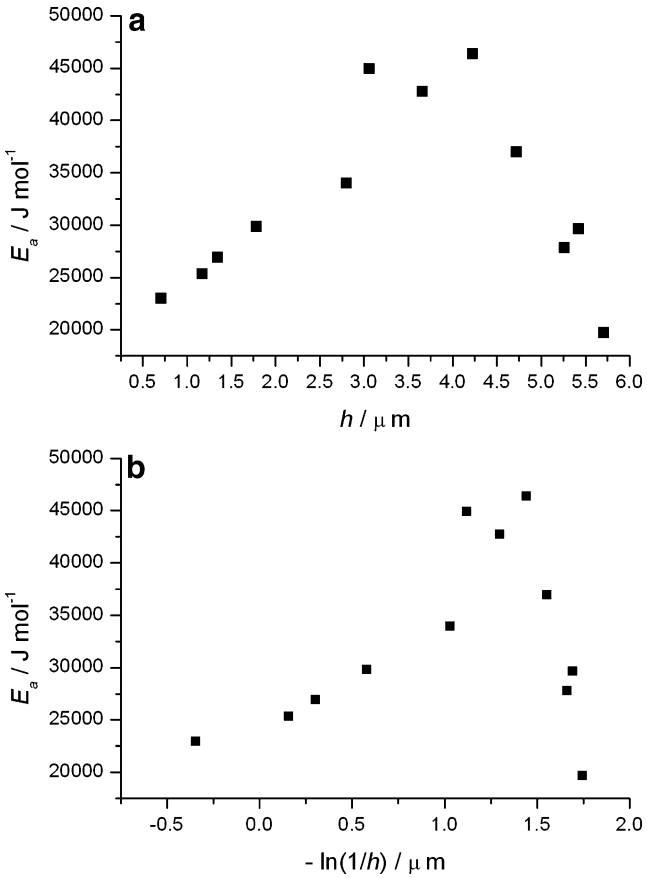

Fig. 5 **a** Evolution of the activation energy (E_a) as a function of the film thickness. **b** Semilogarithmic plot of the inverse of the thickness vs. the activation energy

obtained from polybithiophene films by impedance measurements changes with the film thickness showing two different regions [64]. From the chronoamperometric results, the ESCR model allows the obtention of diffusion coefficients for the studied thicknesses and temperatures [30, 65, 66].

To quantify the speed of the oxidation reaction, stretched exponential curves can be used to fit the anodic chronoamperograms [67].

The stretched exponential function is given by [68, 69]

$$I = I_0 e^{(-t/\tau)^{\beta}};\ 0 < \beta < 1 \tag{10}$$

where I is the current, I_0 is the initial current, τ is a relaxation time, t is the elapsed time, and β is the stretching

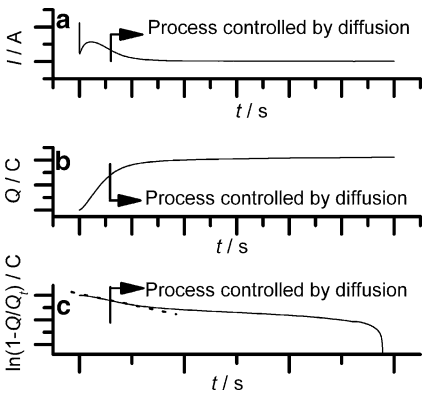

Fig. 6 Treatment of the experimental results to obtain the diffusion coefficients. **a** Experimental oxidation chronoamperogram. **b** Oxidation chronocoulogram obtained by integration of the chronoamperogram showed in **a**. **c** ln $(1-Q/Q_t)$ vs. t obtained from **b**. The reaction time for starting diffusion kinetic control is indicated on every figure

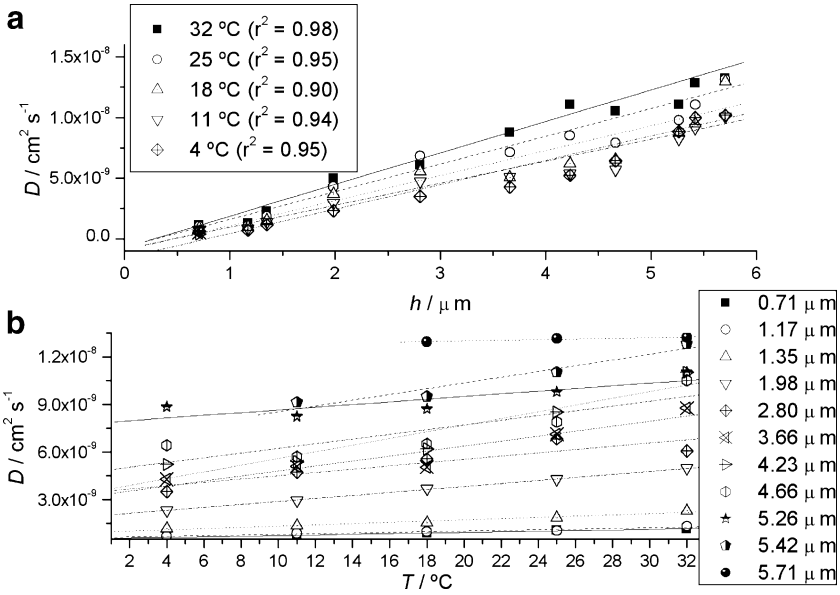

Fig. 7 **a** Diffusion coefficients as a function of the film thicknesses at different temperatures. **b** Diffusion coefficients as a function of the temperature for different film thicknesses

coefficient. Stretched exponentials have been used to fit a range of relaxation behaviors in disordered and non-equilibrium systems [70–72], with β being an empirical value [73].

Of relevance to its use herewith pPy redox, such a function can be used to describe a system with a distribution of relaxation times, for example due to different local environments or conjugation lengths.

The empirical stretched exponentials were deduced by the first time on a physical chemical bases by the ESCR, describing the chronoamperometric results from conjugated polymers when the redox process occurs under diffusion kinetic control [74].

It should be noted that when β=1, such a fit corresponds to any part of the chronoamperogram occurring in absence of conformational relaxation control [30]:

$$I_d(t) = bQ_d e^{-bt} \tag{11}$$

Table 1 Slopes and origin ordinates obtained by linear regressions from the plot of the diffusion coefficient vs. the square of the films thickness

T (ºC)	h^2		
	Slope ($cm^2s^{-1}\mu m^{-1}$)	Origin ordinate (cm^2s^{-1})	r^2
4	$5.90\ 10^{-10}$	$3.29\ 10^{-10}$	0.98
11	$1.16\ 10^{-9}$	$2.91\ 10^{-10}$	0.95
18	$1.29\ 10^{-9}$	$3.33\ 10^{-10}$	0.91
25	$1.95\ 10^{-9}$	$3.59\ 10^{-10}$	0.91
32	$2.34\ 10^{-9}$	$4.04\ 10^{-10}$	0.92

Under those conditions, the total oxidation charge and the charge consumed at any oxidation time, t, after the potential step are related by:

$$\ln[1 - Q/Q_t] = -bt \tag{12}$$

where the diffusion coefficient, D, from the solution, across the already oxidized material toward the film oxidation front is included by b:

$$D = bh^2/2 \tag{13}$$

where h is the thickness of the polymeric film. The constant b can be obtaining by plotting ln $(1-Q/Q_t)$ vs. t, once the conformational relaxation kinetic control along the chronoamperograms has finished; Q is the charge consumed at

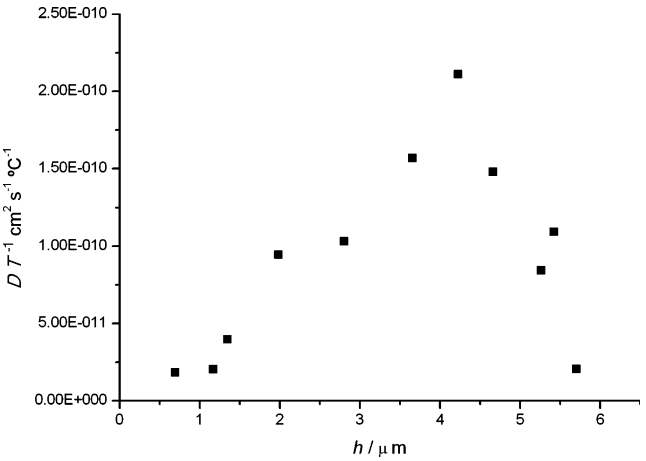

Fig. 8 Slopes obtained by linear regression of the lines shown in Fig. 7b for different thickness of the polypyrrole films

every time t after the potential step; and Q_t is the total charge obtained by integration of the complete chronoamperograms. This procedure is shown in Fig. 6.

For every temperature, the slope obtained from the plot $\ln(1-Q/Q_t)$ vs. t, in the region where the diffusion is the predominant process, is the constant b, allowing the obtention of the diffusion coefficient, D, of the counterions across the swelling polymer during the oxidation process.

Increasing diffusion coefficients are obtained for increasing polymer thicknesses (Fig. 7a), giving linear dependencies with the square of the film thickness as predicted by Eq. 13. Table 1 shows slopes, origin ordinates, and correlation coefficients for the representation of D vs. h^2 following Eq. 13.

The diffusion coefficient for every film thickness increases linearly with temperature (Fig. 7b). For these linear regressions slopes represent the variation of the diffusion coefficient per degree of temperature (D/T, as $cm^2\ s^{-1}{}^{\circ}C^{-1}$) for each of the studied film thicknesses.

Figure 8 shows the evolution of this diffusion coefficient per degree of temperature, as a function of the film thickness. This evolution is parallel to that of the activation energy with the film thickness. The diffusion coefficient of counterions inside the swelling polymer film is related to the film molecular packing structure [65, 66]. Temperature also influence conformational movements rate. In this way, results from Fig. 8 point to a change on the average molecular structure of the film for thicker films than 4 μm. Under this structural picture results from Figs. 5 and 8 point to a possible change of the molecular structure (decreasing cross-linking, branching points, and/or degradation points along the chains) for films thicker than 4 μm obtained during film's electrogeneration.

This interpretation should be supported by the fact that the kinetic studies of the film electrogeneration support the simultaneous presence of polymerization and degradation processes (understood as cross-linking, branching, and nucleophyilic attacks) promoted by simultaneous solvent or contaminants oxidation on the platinum electrode [75–77]. The relative weight of those parallel reactions will decrease for rising film thicknesses: the monomer oxidation–polymerization occurs at the polymer–solution interface and the solvent or contaminants discharge at the Pt–polymer interface. The accessibility of this interface to water or contaminants decreases for rising film thicknesses.

Conclusion

As conclusion, at the chronoamperometric maxima the potentiostatic oxidation of polypyrrole films in acetonitrile solutions occurs under kinetic control of the reaction. At different temperatures, the reaction rate follows the expected Arrhenius expression, allowing the obtention of the activation energy for the full process.

The activation energy for the oxidation of polypyrrole films in acetonitrile solution presents two different regions as a function of the film thickness. The activation energy increases when the thickness rises up to 4 μm, then the activation energy decreases for increasing thicknesses.

The diffusion coefficient of the counterions inside the swelling material required to complete the oxidation process increases as a function of both film thickness and temperature. The variation of the diffusion coefficient per degree of temperature as a function of the film thickness is similar of that found for the activation energy, presenting the same two regions.

A change of the film molecular structure is proposed to occur during the electropolymerization time: more rigid, cross-linked and branched for thinner films (<4 μm), and with longer, non-degraded, chains for thicker films.

Acknowledgments Authors acknowledge financial support from Spanish Government (MCI) Projects MAT2008-06702, Seneca Foundation Project 08684/PI/08, Consejería de Educación de Murcia, and Plan Regional de Ciencia y Tecnología 2007–2010.

References

1. Burgmayer P, Murray RW (1982) An ion gate membrane—electrochemical control of ion permeability through a membrane with an embedded electrode. J Am Chem Soc 104:6139–6140
2. Burgmayer P, Murray RW (1983) Ion gates—electroactive membranes with embedded electrodes. J Electrochem Soc 130:C117–C117
3. Baughman RH, Shacklette LW, Elsembaumer RL, Plitcha E, Becht C (1990) In: Brédas JL, Chance RR (eds) Conjugated polymer materials. Opportunities in electronics, optoelectronics and molecular electronics. Kluwer Academic Publisher, Netherlands
4. Baughman RH, Shacklette LW (1991) In: Salanek WR, Clark DT, Samuelson EJ (eds) Science and application of conducting polymers. Adam Hilger, Bristol
5. Pei QB, Inganas O (1992) Electrochemical applications of the bending beam method. 1. Mass-transport and volume changes in polypyrrole during redox. J Phys Chem 96:10507–10514
6. Burgmayer P, Murray RW (1984) Ion gate electrodes—polypyrrole as a switchable ion conductor membrane. J Phys Chem 88:2515–2521
7. Mermilliod N, Zuppiroli L, Francois B (1982) Swelling of polyacetylene when doped with iodine or sodium. Mol Cryst Liq Cryst 86:1971–1971
8. Francois B, Mermilliod N, Zuppiroli L (1981) Swelling of polyacetylene when doped by iodine or sodium. Synth Met 4:131–138
9. Okabayashi K, Goto F, Abe K, Yoshida T (1987) Electrochemical studies of polyaniline and its application. Synth Met 18:365–370
10. Okabayashi K, Goto F, Abe K, Yoshida T (1989) In situ electrogravimetric analysis of polypyrrole and polyaniline positive electrodes in nonaqueous medium. J Electrochem Soc 136:1986–1988
11. Slama M, Tanguy J (1989) Electrogravimetrical study of polypyrrole. Synth Met 28:C171–C176
12. Pei QB, Inganas O (1993) Electrochemical applications of the bending beam method. 2. Electroshrinking and slow relaxation in polypyrrole. J Phys Chem 97:6034–6041

13. Shimoda S, Smela E (1998) The effect of pH on polymerization and volume change in PPy(DBS). Electrochim Acta 44:219–238
14. Smela E, Gadegaard N (2001) Volume change in polypyrrole studied by atomic force microscopy. J Phys Chem B 105:9395–9405
15. Smela E, Gadegaard N (1999) Surprising volume change in PPy (DBS): an atomic force microscopy study. Adv Mater 11:953
16. Lizarraga L, Andrade EM, Molina FV (2004) Swelling and volume changes of polyaniline upon redox switching. J Electroanal Chem 561:127–135
17. Andrade EM, Molina FV, Florit MI, Posadas D (2000) Volume changes of poly(2-methylaniline) upon redox switching—anion and relaxation effects. Electrochem Solid St 3:504–507
18. Chen XW, Inganas O (1995) Doping-induced volume changes in Poly(3-Octylthiophene) solids and gels. Synth Met 74:159–164
19. Barbero C, Kotz R (1994) Nanoscale dimensional changes and optical-properties of polyaniline measured by in-situ spectroscopic ellipsometry. J Electrochem Soc 141:859–865
20. Aldissi M (ed) (1992) Intrinsically conducting polymers: an emerging technology. Kluwer Academic Publishers, Dordrecht
21. Nalwa HS (ed) (1997) Handbook of organic conductive molecules and polymers. Wiley, Chichester
22. De Rossi D, Osada Y (eds) (2010) Polymer sensors and actuators. Springer, Berlin
23. Elices M (ed) (2010) Structural biological materials. Design and structure-properties relationships. Pergamon, Amsterdam
24. Skotheim TA, Reynolds JR (eds) (2006) Handbook of conducting polymers. CRC Press, New York
25. Shahinpoor M, Schneider H-J (eds) (2008) Intelligent materials. RSC, Cambridge
26. Grande H, Otero TF (1999) Conformational movements explain logarithmic relaxation in conducting polymers. Electrochim Acta 44:1893–1900
27. Grande H, Otero TF (1998) Intrinsic asymmetry, hysteresis, and conformational relaxation during redox switching in polypyrrole: a coulovoltametric study. J Phys Chem B 102:7535–7540
28. Grande H, Otero TF, Cantero I (1998) Conformational relaxation in conducting polymers: effect of polymer-solvent interactions. J Non-Cryst Solids 235:619–622
29. Otero TF, Grande H, Rodriguez J (1997) Role of conformational relaxation on the voltammetric behavior of polypyrrole. Experiments and mathematical model. J Phys Chem B 101:8525–8533
30. Otero TF, Grande HJ, Rodriguez J (1997) Reinterpretation of polypyrrole electrochemistry after consideration of conformational relaxation processes. J Phys Chem B 101:3688–3697
31. Otero TF, Grande H (1996) Thermally enhanced conformational relaxation during electrochemical oxidation of polypyrrole. J Electroanal Chem 414:171–176
32. Otero TF, Ariza MJ (2003) Revisiting the electrochemical and polymeric behavior of a polypyrrole free-standing electrode in aqueous solution. J Phys Chem B 107:13954–13961
33. Otero TF (2009) Soft, wet, and reactive polymers. Sensing artificial muscles and conformational energy. J Mater Chem 19:681–689
34. Otero TF, Santos F (2008) Polythiophene oxidation: rate coefficients, activation energy and conformational energies. Electrochim Acta 53:3166–3174
35. Otero TF, de Otazo JMG (2009) Polypyrrole oxidation: kinetic coefficients, activation energy and conformational energy. Synth Met 159:681–688
36. Arias-Pardilla J, Otero TF, Blanco R, Segura JL (2010) Synthesis, electropolymerization and oxidation kinetics of an anthraquinone-functionalized poly(3, 4-ethylenedioxythiophene). Electrochim Acta 55:1535–1542
37. Otero TF, Abadias R (2007) Poly(3-methylthiophene) oxidation under chemical control. Rate coefficients change with prepolarization potentials of reduction. J Electroanal Chem 610:96–101
38. Trueba M, Trasatti SP (2009) Pyrrole-based silane primer for corrosion protection of commercial Al alloys. Part II. Corrosion performance in neutral NaCl solution. Prog Org Coat 66:265–275
39. Truong VT (1992) Thermal-degradation of polypyrrole—effect of temperature and film thickness. Synth Met 52:33–44
40. Harima Y, Kishimoto K, Mizota H (2007) Light reflection at polyaniline films and its application to a kinetic study of polymer chain conformation. Electrochim Acta 53:657–663
41. Mortimer RJ, Graham KR, Grenier CRG, Reynolds JR (2009) Influence of the film thickness and morphology on the colorimetric properties of spray-coated electrochromic disubstituted 3, 4-propylenedioxythiophene polymers. ACS Appl Mater Interfaces 1:2269–2276
42. Barnoss S, Shanak H, Bufon CCB, Heinzel T (2009) Piezoresistance in chemically synthesized polypyrrole thin films. Sensor Actuat A Phys 154:79–84
43. Hu CC, Chu CH (2001) Electrochemical impedance characterization of polyaniline-coated graphite electrodes for electrochemical capacitors—effects of film coverage/thickness and anions. J Electroanal Chem 503:105–116
44. Lissy SLG, Pitchumani S, Jayakumar K (2002) The effect of film thickness and counter ions on the double layer and redox capacitance of polyaniline thin film electrode. Mater Chem Phys 76:143–150
45. Valaski R, Ayoub S, Micaroni L, Hummelgen IA (2002) Influence of film thickness on charge transport of electrodeposited polypyrrole thin films. Thin Solid Films 415:206–210
46. Arenas MA, Bajos LG, de Damborenea JJ, Ocon P (2008) Synthesis and electrochemical evaluation of polypyrrole coatings electrodeposited onto AA-2024 alloy. Prog Org Coat 62:79–86
47. Atta NF, Galal A, Khalifa F (2007) Electrodeposited metals at conducting polymer electrodes I—effect of particle size and film thickness on electrochemical response. Appl Surf Sci 253:4273–4282
48. Ayad MM, Shenashin MA (2003) Film thickness studies for the chemically synthesized conducting polyaniline. Eur Polym J 39:1319–1324
49. Presa MJR, Posadas D, Florit MI (2000) Voltammetric study of the reduction and relaxation of poly(o-toluidine). Effect of the polymer thickness and the external electrolyte nature and concentration. J Electroanal Chem 482:117–124
50. de Torresi SIC, Bassetto AN, Trasferetti BC (1998) Effect of thickness, chemical nature of dopants and an alkyl substituent on absorption bands of polyaniline. J Solid State Electr 2:24–29
51. Shishkanova TV, Matejka P, Kral V, Sedenkova I, Trchova M, Stejskal J (2008) Optimization of the thickness of a conducting polymer, polyaniline, deposited on the surface of poly(vinyl chloride) membranes: a new way to improve their potentiometric response. Anal Chim Acta 624:238–246
52. Stussi E, Stella R, De Rossi D (1997) Chemoresistive conducting polymer-based odour sensors: influence of thickness changes on their sensing properties. Sensor Actuat B Chem 43:180–185
53. Van CN, Potje-Kamloth K (2000) The influence of thickness and preparation temperature of doped polypyrrole films on the electrical and chemical sensing properties of polypyrrole/gold Schottky barrier diodes. J Phys D Appl Phys 33:2230–2238
54. Wiziack NKL, Paterno LG, Fonseca FJ, Mattoso LHC (2007) Effect of film thickness and different electrode geometries on the performance of chemical sensors made of nanostructured conducting polymer films. Sensor Actuat B Chem 122:484–492
55. Gill E, Arshak A, Arshak K, Korostynska O (2009) Effects of polymer binder, surfactant and film thickness on pH sensitivity of polymer thick film sensors. Procedia Chem 1:265–268
56. Shiu KK, Song FY, Lau KW (1999) Effects of polymer thickness on the potentiometric pH responses of polypyrrole modified glassy carbon electrodes. J Electroanal Chem 476:109–117

57. Sundfors F, Bobacka J, Ivaska A, Lewenstam A (2002) Kinetics of electron transfer between Fe(CN)63-/4- and poly(3, 4-ethylenedioxythiophene) studied by electrochemical impedance spectroscopy. Electrochim Acta 47:2245–2251
58. Randriamahazaka H, Plesse C, Teyssiθ D, Chevrot C (2005) Relaxation kinetics of poly(3, 4-ethylenedioxythiophene) in 1-ethyl-3-methylimidazolium bis((trifluoromethyl)sulfonyl)amide ionic liquid during potential step experiments. Electrochim Acta 50:1515–1522
59. Higgins MJ, McGovern ST, Wallace GG (2009) Visualizing dynamic actuation of ultrathin polypyrrole films. Langmuir 25:3627–3633
60. Otero TF, Carrasco J, Figueras A, Brillas E (1996) Electrogeneration of poly(2, 5-di-(2-thienyl)-pyrrole) in acetonitrile. Kinetics, productivity and composition of the oxidized form. Synth Met 83:193–196
61. Atkins PW, Depaula J (2001) Physical chemistry. W H Freeman & Co., New York
62. Otero TF, Abadias R (2008) Potentiostatic oxidation of poly(3-methylthiophene): influence of the prepolarization time at cathodic potentials on the kinetics. J Electroanal Chem 618:39–44
63. Garcia-Belmonte G, Bisquert J (2002) Impedance analysis of galvanostatically synthesized polypyrrole films. Correlation of ionic diffusion and capacitance parameters with the electrode morphology. Electrochim Acta 47:4263–4272
64. Popkirov GS, Barsoukov E, Schindler RN (1997) Investigation of conducting polymer electrodes by impedance spectroscopy during electropolymerization under galvanostatic conditions. J Electroanal Chem 425:209–216
65. Suarez IJ, Otero TF, Marquez M (2005) Diffusion coefficients in swelling polypyrrole: ESCR and Cottrell models. J Phys Chem B 109:1723–1729
66. Otero TF, Marquez M, Suarez IJ (2004) Polypyrrole: diffusion coefficients and degradation by overoxidation. J Phys Chem B 108:15429–15433
67. West BJ, Otero TF, Shapiro B, Smela E (2009) Chronoamperometric study of conformational relaxation in PPy(DBS). J Phys Chem B 113:1277–1293
68. Ariza MJ, Otero TF (2005) Ionic diffusion across oxidized polypyrrole membranes and during oxidation of the free-standing film. Colloids Surf A 270:226–231
69. Bendler JT, Fontanella JJ, Shlesinger MF (2007) Anomalous diffusion producing normal relaxation and transport. J Phys Condens Matter 19:065121–065121
70. Lee KCB, Siegel J, Webb SED, Leveque-Fort S, Cole MJ, Jones R, Dowling K, Lever MJ, French PMW (2001) Application of the stretched exponential function to fluorescence lifetime imaging. Biophys J 81:1265–1274
71. Lin FD, Wang YJ, Lonergan M (2008) Ion transport in polyacetylene ionomers. J Appl Phys 104:103517–103517
72. Funston AM, Fadeeva TA, Wishart JF, Castner EW (2007) Fluorescence probing of temperature-dependent dynamics and friction in ionic liquid local environments. J Phys Chem B 111:4963–4977
73. Stretched exponential functions (2008) Wikipedia. http://en.wikipedia.org/wiki/Stretched_exponential_function. Accessed 22 June 2010
74. Otero TF, Boyano I (2003) Comparative study of conducting polymers by the ESCR model. J Phys Chem B 107:6730–6738
75. Otero TF, Santamaria C (1991) Polypyrrole electrogeneration at different potentials—ex situ microgravimetric control. J Electroanal Chem 312:285–291
76. Otero TF, Rodriguez J (1994) Parallel kinetic-studies of the electrogeneration of conducting polymers—mixed materials, composition and properties control. Electrochim Acta 39:245–253
77. Otero TF (1999) In: White RE (ed) Modern aspects of electrochemistry. Kluwer Academic, Plenum Publishers, New York, pp 307–432